

Article

Molecular Dynamics Study of Friction between Ag Nanoparticle and Two-Dimensional Titanium Carbide Ti₂C (MXene)

Vadym Borysiuk^{1,2,*}, Iakov A. Lyashenko¹  and Valentin L. Popov^{1,3} 

¹ Department of System Dynamics and Friction Physics, Institute of Mechanics, Technische Universität Berlin, 10623 Berlin, Germany; i.lyashenko@tu-berlin.de (I.A.L.); v.popov@tu-berlin.de (V.L.P.)

² Department of Computerized Control Systems, Faculty of Electronics and Information Technology, Sumy State University, 40007 Sumy, Ukraine

³ Samarkand State University, Samarkand 140104, Uzbekistan

* Correspondence: v.borysiuk@campus.tu-berlin.de; Tel.: +49-(0)30-314-75917

Abstract: We report the results of atomistic simulations of friction between two-dimensional titanium carbide Ti₂C (MXene) and a silver nanoparticle located on its surface. Numerical experiments were performed within classical molecular dynamics methods using a previously developed scheme for simulations of interactions between MXenes and metal nanoparticles. In the computer experiments performed, both tangential and shear forces were applied to the Ag nanoparticle to initiate its sliding on the surface of the Ti₂C MXene. During the simulations, the nanotribological parameters of the studied system, such as the friction force, contact area, friction coefficient, and tangential shear, were computed. It is shown that, for the studied system, the friction coefficient does not depend on the velocity of nanoparticle movement or the contact area. Additionally, the sliding friction of the nanoparticle on the flexible substrate was considered. The latter case is characterized by a larger friction coefficient and contact area due to the formation of wrinkles on the surface of the substrate.

Keywords: nanoparticle; 2D crystal; MXene; molecular dynamics; simulations; friction coefficient; contact area



Citation: Borysiuk, V.; Lyashenko, I.A.; Popov, V.L. Molecular Dynamics Study of Friction between Ag Nanoparticle and Two-Dimensional Titanium Carbide Ti₂C (MXene). *Crystals* **2024**, *14*, 272. <https://doi.org/10.3390/cryst14030272>

Academic Editors: Bosong Sun and Kwun Nam Hui

Received: 20 January 2024

Revised: 24 February 2024

Accepted: 1 March 2024

Published: 12 March 2024



Copyright: © 2024 by the authors. Licensee MDPI, Basel, Switzerland. This article is an open access article distributed under the terms and conditions of the Creative Commons Attribution (CC BY) license (<https://creativecommons.org/licenses/by/4.0/>).

1. Introduction

Studying friction and wear at an atomic scale is one of the most popular topics of research among various scientific groups working in the field of nanotechnologies [1–3]. Understanding interatomic friction became especially important for the design and technological application of various nanoelectromechanical systems (NEMs) with moving components, as it may help to significantly increase their reliability and ensure proper functioning [4–8].

Besides technological nanodevices, understanding friction at an atomic scale is also important for the fabrication of various hybrid nanomaterials, especially for the decoration of two-dimensional (2D) crystals with nanoparticles (NPs) [9,10]. Such composites are created to improve the performance of 2D materials and for further use as components of nanoelectronics and various NEMS devices. As expected, the most intensively studied 2D material for such hybrids is graphene. Various examples of chemical modification of graphene with metal nanoparticles exist in the literature. For instance, the decoration of single-layer graphene sheets with nickel nanoparticles demonstrated an enhanced adsorption of molecular hydrogen [11], and gold-nanoparticle-decorated graphene is used for efficient NO₂ gas sensing [12] and surface-enhanced Raman scattering (SERS) [13]. Compositions of graphene and silver nanoparticles are typically used in (but not limited to) nanoelectronics and various biomedical applications [14,15].

Moreover, composites of nanoparticles and other 2D materials, aside from graphene, are also fabricated and studied intensively. In particular, hybrids of noble metal nanoparticles and two-dimensional titanium carbides, so-called MXenes, were produced recently [16,17]. MXenes are transition-metal carbides and nitrides that have thicknesses from three to seven

atomic planes with extraordinary physical and electrochemical properties, which, together with their unique two-dimensional structure, make them promising materials for various nanotechnological applications [16–20]. Thus, Ref. [16] reports on the production of MXene/Ag composites for lithium-ion batteries, which demonstrate an increased charge rate and number of charge/discharge cycles, while in [17], the authors created hybrid samples of MXenes decorated with silver, gold, or palladium nanoparticles for surface-enhanced Raman spectroscopy.

Naturally, syntheses of hybrid nanomaterials based on noble metal nanoparticles and two-dimensional crystals, including MXenes, have encouraged further studies of adhesion and friction between these nanostructures. It is worth mentioning that the experimental investigation of nanotribological systems may become a hard challenge due to the small sizes of the studied objects and the magnitudes of the friction forces that may appear in the system. Typically, such experiments require special laboratory equipment, such as an atomic force microscope (AFM) [3], a surface force apparatus (SFA) [21], a special type of tribometer, and others. Nevertheless, the number of studies on the friction properties of 2D MXenes reported in the literature is rapidly increasing (see [22] and related references). In addition, nanotribological systems are also intensively studied by various theoretical and computational methods [2,23]. One of the most popular numerical approaches for studying friction during mechanical contacts at the atomistic level is classical molecular dynamics (MD) simulations [24]. In recent years, this approach has been adopted by numerous scientific groups for studying friction between 2D graphene sheets and nanoparticles [25–29]. In the proposed study, we report the results of computer experiments concerning sliding friction between a silver nanoparticle and a two-dimensional Ti₂C sheet performed within the classical MD technique using an adopted numerical scheme that was proposed earlier to study friction between 2D graphene and metal nanoparticles [30].

2. Materials and Methods

In this study, we considered a nanotribological system, which consisted of a silver nanoparticle with a diameter of approximately 2 nm located at the surface of a Ti₂C substrate with lateral sizes of 17 × 39 nm. The snapshots of the initial configuration of the studied system are shown in Figure 1 (all snapshots of atomistic configurations were prepared with the Visual molecular dynamics (VMD) software [31]). The number of Ag atoms in the NP was 512, while the total number of particles involved in the simulation was $\sim 25 \times 10^3$. A previously developed approach based on a combination of interatomic potentials was used for the calculation of interactional forces between carbon and titanium atoms within a Ti₂C sample [32]. Namely, a combination of Lennard–Jones (LJ) and Axilrod–Teller [33–35] potentials was used to describe the interaction between titanium and carbon atoms within the Ti₂C sample, while Ti–Ti interactions within the substrate as well as Ag–Ag interactions in the silver nanoparticle were described within the embedded atom method (EAM) [36]. The forces between the nanoparticle and the substrate were also calculated from the LJ potential [30,37]. A description of the used potentials and numerical values of its parameters are specified in Supplementary file Data S3. We used in-house code that was implemented using the NVIDIA CUDA platform [38,39] for parallel computing on the GPU. Equations of motion were integrated using the velocity Verlet algorithm with a time step of $dt = 0.2$ fs. A description of the model for the interaction between Ag atoms and MXene, as well as other details of the simulation setup, can be found in [10].

We used the model sample of silver NP that was obtained by the deposition of Ag atoms onto the surface of Ti₂C MXene. Details of simulations of the deposition process and a description of the nanoparticle formation can be found in [10]. The obtained silver NP was placed onto the surface of a large MXene nanosheet that was previously relaxed. In our experiments, we considered two separate cases with different constraints. In the first case, periodic and free boundary conditions were applied to the system in the xy plane and z direction, respectively (see Figure 1). At the same time, Ti atoms in the bottom Ti plane of the Ti₂C sheet were not allowed to move in the z direction, while relaxation in

the xy plane was allowed. These conditions prevented the system from shifting in the normal direction and related to experiments with a rigid substrate. In another case, all the atoms in the studied systems were allowed to move in any direction, with periodic and free boundary conditions in the xy plane and z direction, respectively, as in the first case. The system temperature was maintained at 300 K by a Berendsen thermostat [40] in both considered cases.

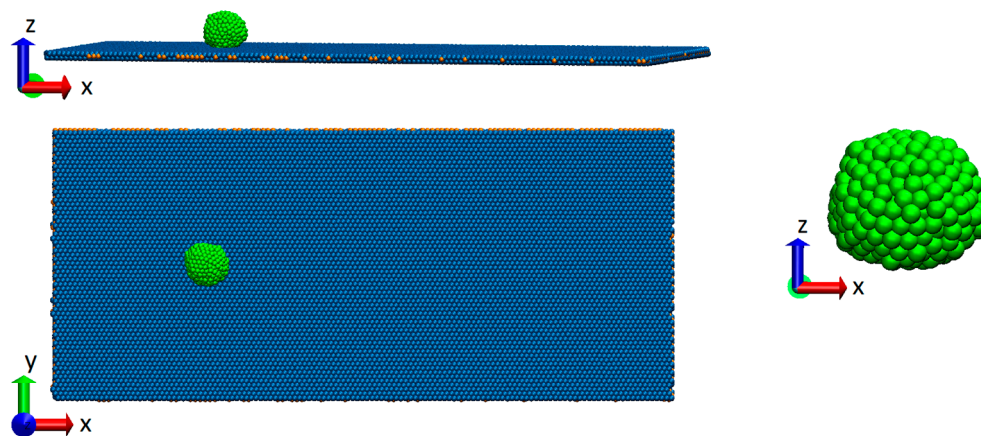


Figure 1. Snapshots (top and perspective view) of the initial configuration of the studied system that consisted of a 2D Ti_2C substrate with Ag nanoparticle on its surface. Right panel of the figure shows the enlarged silver nanoparticle without a substrate. Here and below, Ag atoms are shown in green color, while Ti at C atoms are shown in blue and orange, respectively.

It is worth mentioning that the preliminary study of the interactions between Ag nanoparticles and Ti_2C MXene were also performed in [10]. However, the mentioned study focuses on the deposition process and formation of Ag nanoparticles and nanoislands on the surface of the Ti_2C substrate as well as on measuring the adhesion forces between the NP and substrate in the static case. In addition, the application of an external force to the NP and its sliding were considered for a relatively short time interval due to the small size of the substrate and with a single magnitude of the velocity of the NP's movement. Moreover, the performed experiment was affected by the curved shape of the MXene sheet, which was deformed during the deposition process [10]. Therefore, additional experiments with different magnitudes of the external force applied in the normal and tangential directions were necessary for the fundamental understanding of the friction between the Ag nanoparticle and Ti_2C MXene.

In the performed studies, we adopted a numerical algorithm that imitates standard experiments on sliding friction with a tribometer [41]. According to the common method for tribological experiments with bulk materials, the friction force was measured by a force sensor through the application of an external load to the sample in both the normal and tangential directions. Similarly, we performed a series of computer experiments, where normal and tangential forces of different magnitudes were applied to the silver nanoparticle located at the surface of the 2D MXene sheet, according to algorithm described in [10]. Namely, after calculating the interatomic forces between all the atoms in the system from the MD potentials, additional constant values were added to either the z or x component of the acceleration of the Ag atoms in the nanoparticle for a normal or tangential load, respectively. The computer experiments were performed as follows. After the initial relaxation of the studied system, an external force in the $-z$ direction (see Figure 1) was applied to the silver nanoparticle for 5×10^5 time steps to let the Ag atoms reach a stationary configuration. The normal load applied to the Ag atoms resulted in the slight compression of the NP and an increase in the contact area between the NP and the substrate. It is worth noting that in molecular dynamics simulations, it is convenient to use rescaled units for physical quantities instead of SI units; therefore, we plotted some measured parameters in MD units for an appropriate appearance. Four different magnitudes of the external normal load were

considered in the experiments. For every subsequent experiment, its value was increased by a factor of 2, i.e., $F_N = F_0, 2F_0, 4F_0$, and $8F_0$, where F_0 is the total force that was added to all the Ag atoms in the NP, approximately equivalent to a 5 nN external load. The time dependencies of an average normal coordinate of the nanoparticle during the compression under the external load are shown in Figure 2a.

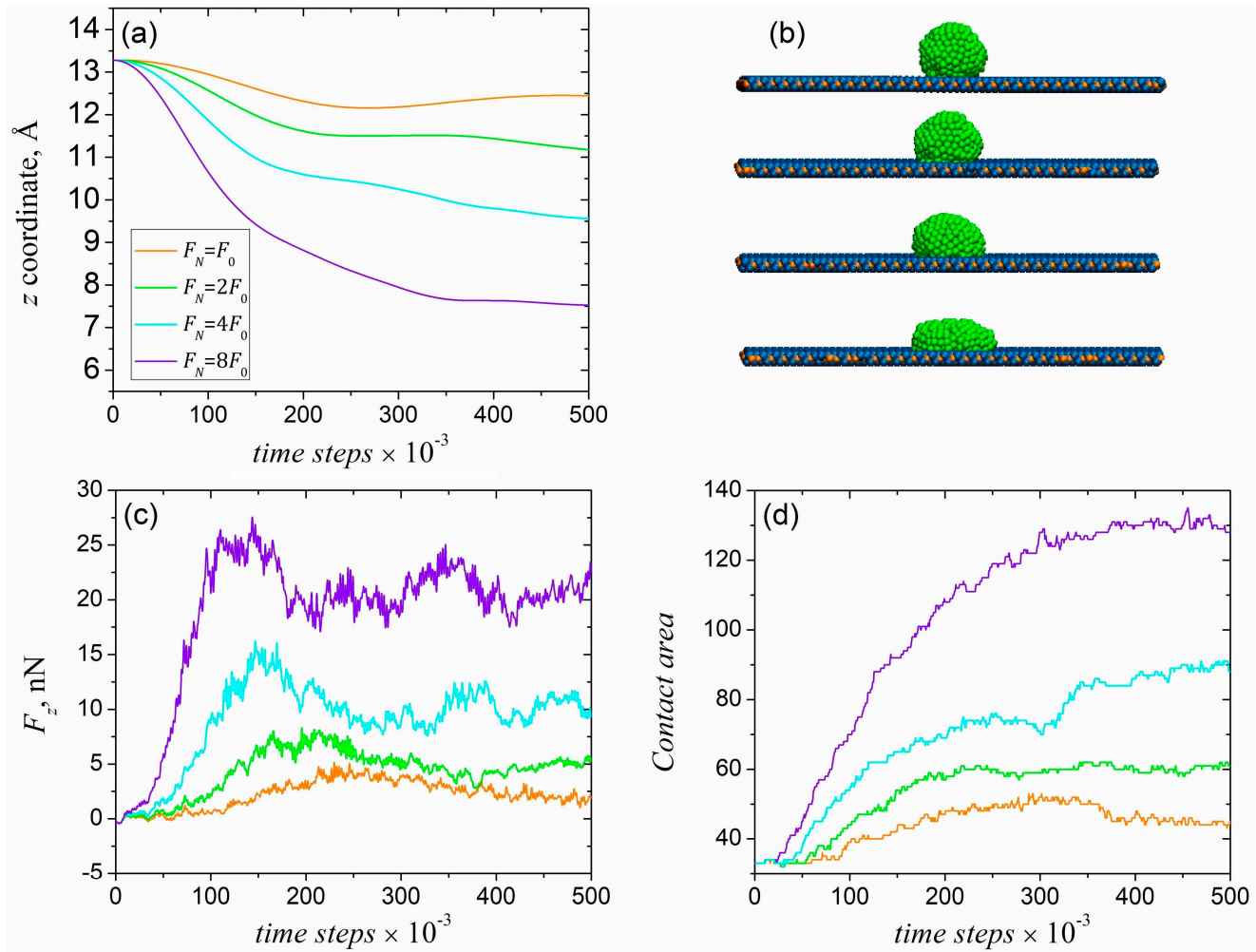


Figure 2. (a) Time dependencies of the average z coordinate of the nanoparticle during application of the external normal load in $-z$ direction. Different colors denote four different magnitudes of the external force (values are shown in the figure). (b) Snapshots of atomistic configurations of the system under external load at the end of each experiment; snapshots from top to bottom are related to final point $t = 500 \times 10^3$ of dependencies $F_N = F_0, 2F_0, 4F_0$, and $8F_0$ in panel (a), respectively. (c) Time dependencies of the normal force acting on the nanoparticle from the substrate during the external load for all experiments. (d) Related time dependencies of the contact area between the nanoparticle and the substrate. Legend and coloring are the same for all panels. Supplementary Video S1 is available.

As it follows from the figure, the largest deformation $\Delta z \approx 0.5$ nm was observed for the maximal applied normal load $8F_0$. Figure 2b shows snapshots of the atomistic configurations of the nanoparticle under different magnitudes of the normal load at the end of each experiment. Namely, each snapshot from top to bottom relates to the experiment with $F_N = F_0, 2F_0, 4F_0$, and $8F_0$, respectively, and it was taken at the point $t = 500 \times 10^3$ from the dependencies shown in Figure 2a (see also Figure 2c,d). It is clearly visible that under the external load, the Ag atoms in the nanoparticle rearranged from their stationary positions, and the NP obtained a more flattered shape compared to its initial configuration.

Figure 2c shows the time dependencies of the z component of the force that acted from the substrate to the NP during the application of the external force to the NP. After an initial short drop to negative values, which was related to attraction between the NP and the substrate, the magnitude of the acting F_z force was always positive, i.e., the force is directed towards the NP in the $+z$ direction. All the presented $F_z(t)$ curves have a typical form, with initial rapid growth and subsequent fluctuations around stationary values. Such behavior relates to the initial compression of the NP and the subsequent relaxation of the Ag atoms to the stationary positions. The height of the initial peak and the growth rate of all the presented dependencies were proportional to the magnitude of the applied external load. As mentioned above, the applied load was multiplied by a factor of 2 in each subsequent experiment; correspondingly, the stationary values of the response from the substrate also approximately differed by a factor of 2. However, in the simulations, the measured reaction from the substrate was not exactly equal to the force applied to the NP due to the boundary constraints in the z direction and the applied thermostat algorithm. Nevertheless, such an approach for measuring forces that act in the system is qualitatively correct and commonly used in simulations [30].

The application of the external force to the nanoparticle also caused a growth in the contact area between the nanoparticle and the substrate. In our simulations, we measured the size of the contact area as the number of atoms in the top plane of the Ti_2C substrate that were in direct contact with the Ag atoms in the nanoparticle (substrate and NP atoms were considered to be in direct contact if the distance between them was within 4 Å). Even though number of atoms in the contact can be transferred to standard m^2 , such a measuring unit is more convenient and was appropriate to use in the simulations, as we did not aim to obtain exact values of the numerical parameters of the system but rather to obtain a qualitative picture of the physical processes that appeared on an atomistic level. It is also worth noting that the contact area in MD simulations can be defined in an alternative way, for example, using the lateral dimensions of the nanoparticle and approximating it with ellipse (see [30]). Figure 2d shows the time dependencies of the contact area size during the compression. The presented dependencies were similar to the corresponding $F_z(t)$ curves and were characterized by fast initial growth and subsequent fluctuations around stationary values. As expected, the increment in the size of the contact area by the end of the experiments was proportional to the magnitude of the applied normal load, which was also confirmed by the visual analysis of the snapshots shown in Figure 2b and Supplementary Video S1.

After reaching the stationary state under the normal load, the tangential force in the $+x$ direction, to which we will also refer as a shear force, was applied to the NP via the same algorithm as the normal force. During the simulation, the friction force, position, and velocities of the NP as well as the size of the contact area between the NP and the substrate were computed. The results of performed experiments are presented in the following section.

3. Results and Discussion

As mentioned above, we conducted a series of tribological experiments with different magnitudes of the external load. Hence, we performed simulations where tangential external forces of the same magnitude were applied to the NP in the $+x$ direction together with four different magnitudes of the normal load, as described in the previous section. For every experiment with the shear force, the starting point of the system was related to the final point (5×10^5 time steps) after the compression procedure (see Figure 2), with the same value of the external normal force acting on the nanoparticle. The application of the external tangential force resulted in translational motion of the nanoparticle. During the NP motion in the $+x$ direction, its x coordinate was recorded as an average value of all the x coordinates of the Ag atoms. Further, the velocity of the nanoparticle motion was calculated as the derivative of its coordinate with respect to time. The obtained dependencies are shown in Figure 3a,b respectively.

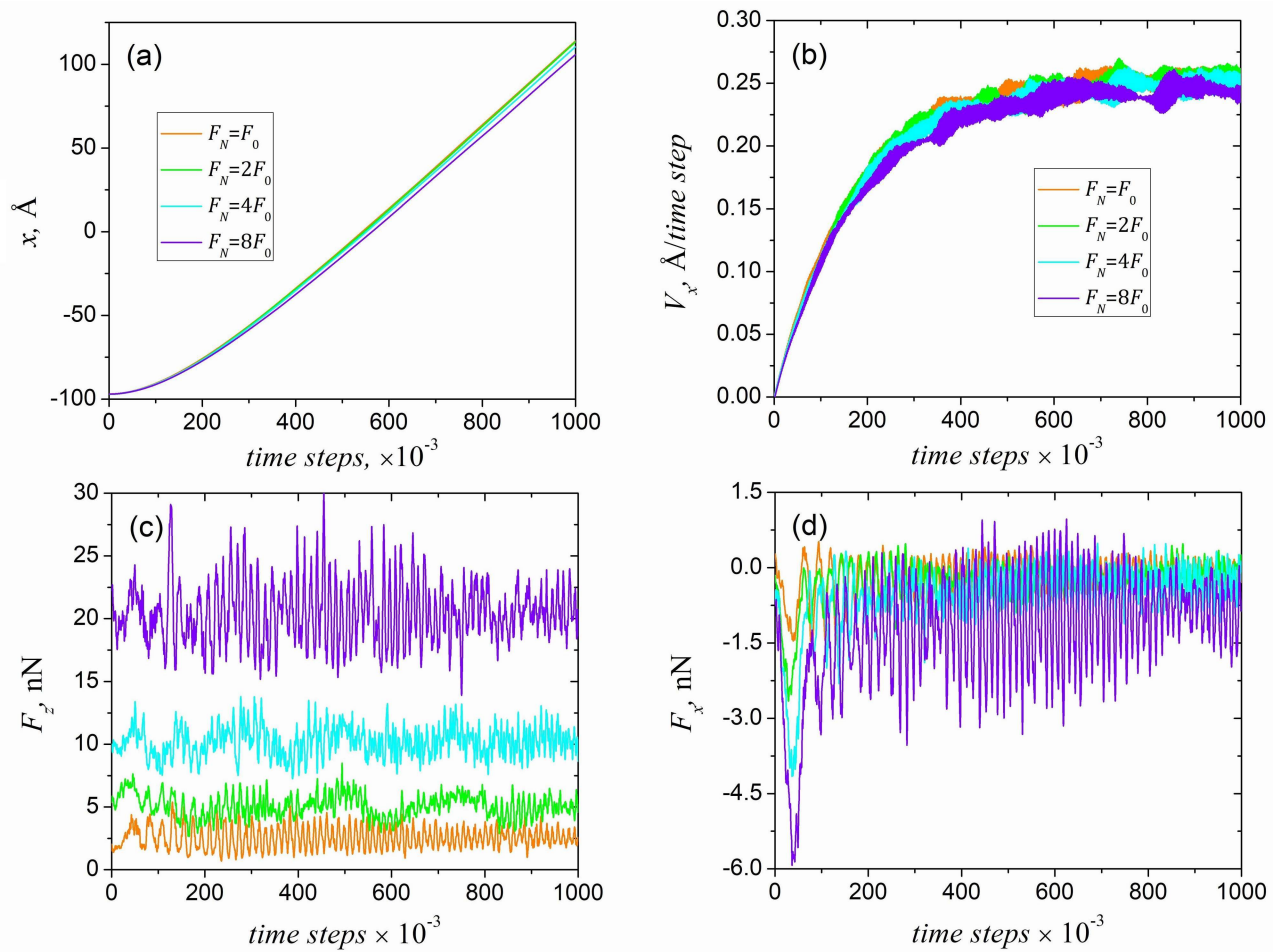


Figure 3. (a) Time dependencies of the average x coordinate of the nanoparticle during application of the external shear force in $+x$ direction. Different colors denote four different magnitudes of the external load (values are shown in the figure). (b) Time dependencies of the x components of the NP velocities obtained from the time dependencies of coordinates from panel (a). (c,d) Related time dependencies of the normal F_z and tangential F_x forces acting on the nanoparticle from the substrate. Legend and coloring are the same for all panels.

As follows from the presented data, the velocity of the NP motion almost did not depend on the normal load. Also, the acceleration of the nanoparticle continued for approximately half of the simulation time, and after this, the velocity of the NP did not increase monotonically, while it continued to fluctuate around its stationary value. During the sliding of the nanoparticle, we recorded the normal components of the forces that acted on the NP from the substrate, which were necessary for the determination of the friction coefficient. The time dependencies of these forces are shown in Figure 2c. As can be seen in the figure, the normal response from the substrate generally preserved its initial value that was acting in the system before the application of the shear force. However, the $F_z(t)$ dependencies fluctuated around these values with an almost constant amplitude for each case during the whole experiment. In addition, we computed the friction force between the nanoparticle and the substrate. In our experiments, we defined the friction force as the x component of the total force that acted from the substrate to the Ag atoms in the nanoparticle [30]. The obtained dependencies are shown in Figure 3d. All the presented curves are characterized by a sharp drop to negative values at the start of simulation, when the external shear force appeared in the system, which was related to a prompt increase in the friction with the beginning of the NP's motion (since the NP moved in the $+x$ direction, the friction force was negative, i.e., $F_x < 0$). As was reported in our previous study [10], translational motion of the silver nanoparticle on the surface of the MXene substrate began

when a certain critical value of the shear force F_c was applied to the NP. The magnitude of this critical force depends on the particular configuration of the studied system. Here, we only considered shear force values that were greater than the critical value, as our aim was to study sliding friction of the NP. Thus, the interaction force between the NP and the substrate reached its maximal value just before the NP began to slide continuously on the substrate. However, according to Figure 3a,b, the average x coordinate of the NP and the related velocity may already have had nonzero values before the actual motion of the NP due to the shift in some Ag atoms within the nanoparticle without the movement of the NP as whole. The amplitude of the opening peak in the $F_x(t)$ dependencies, which is related to the static friction force, may be considered as a critical shear force that is needed to initiate the NP's motion. This situation is typical for different tribological systems [42,43] and is qualitatively correct. As follows from the obtained data, the critical value of the shear force varied for each experiment and increased with the growth of the external normal load. In general, within MD simulations, static friction may also depend on the particular atomistic configuration of the system and the number of contacting atoms. After the initial peak, the $F_x(t)$ dependencies relaxed to a certain magnitude, that is, $F_x < 0$, and continued to fluctuate around these values. Such fluctuations in the force between the NP and the substrate during sliding may be caused by motion within the periodic potential due the arrangement of the substrate atoms into a crystal lattice [30]. Examples of the evolution of the atomistic configuration of the system and the contact area under shear force are presented in Supplementary Video S2.

To study the properties of the system at different velocities of movement, we also performed experiments with different magnitudes of the shear force while a constant normal load $F_N = F_0$ was applied to the nanoparticle. The results of the performed experiments are shown in Figure 4. As follows from the figure, the time dependencies of the x coordinates and the velocities of the NP (Figure 4a,b) had a similar form to the previous case with different normal load magnitudes (see Figure 3a,b). At the same time, each magnitude of the applied shear force resulted in a different stationary value of the established velocity of the NP. It is worth noting that the top curves in Figure 2a,b end earlier than the bottom dependencies. This situation was caused by the fact that the $F_s = 20F_0$ curves are related to the maximal observed velocity of the NP, and in this case, the nanoparticle reached the end of the substrate before the final time of the experiment (earlier 10^6 time steps). The time dependencies of the normal force acting on the NP from the substrate, as shown in Figure 4c, were equivalent due to the same magnitude of the normal load applied to the nanoparticle. At the same time, the measured friction force also did not depend on the nanoparticle velocity, as follows from the overlapping dependencies $F_x(t)$ for different shear forces, as shown in Figure 4c.

To obtain the quantitative characteristics of the studied system, we also computed the friction coefficients for all the considered cases according to standard definition $\mu = F_x/F_z$ from the data shown in Figures 3 and 4. It is worth noting that the time dependencies of the normal and tangential forces presented above were characterized by the presence of strong fluctuations and relatively close magnitudes, which made it difficult to distinguish the data from the separate experiments. To make the obtained dependencies more apparent, we calculated the average values of the friction coefficients using a moving average filter. The results of these calculations are presented in Figure 5. The obtained dependencies were similar for all the considered cases, with an initial relaxation and subsequent fluctuations around stationary values in the range $\mu = 0.02$ – 0.05 .

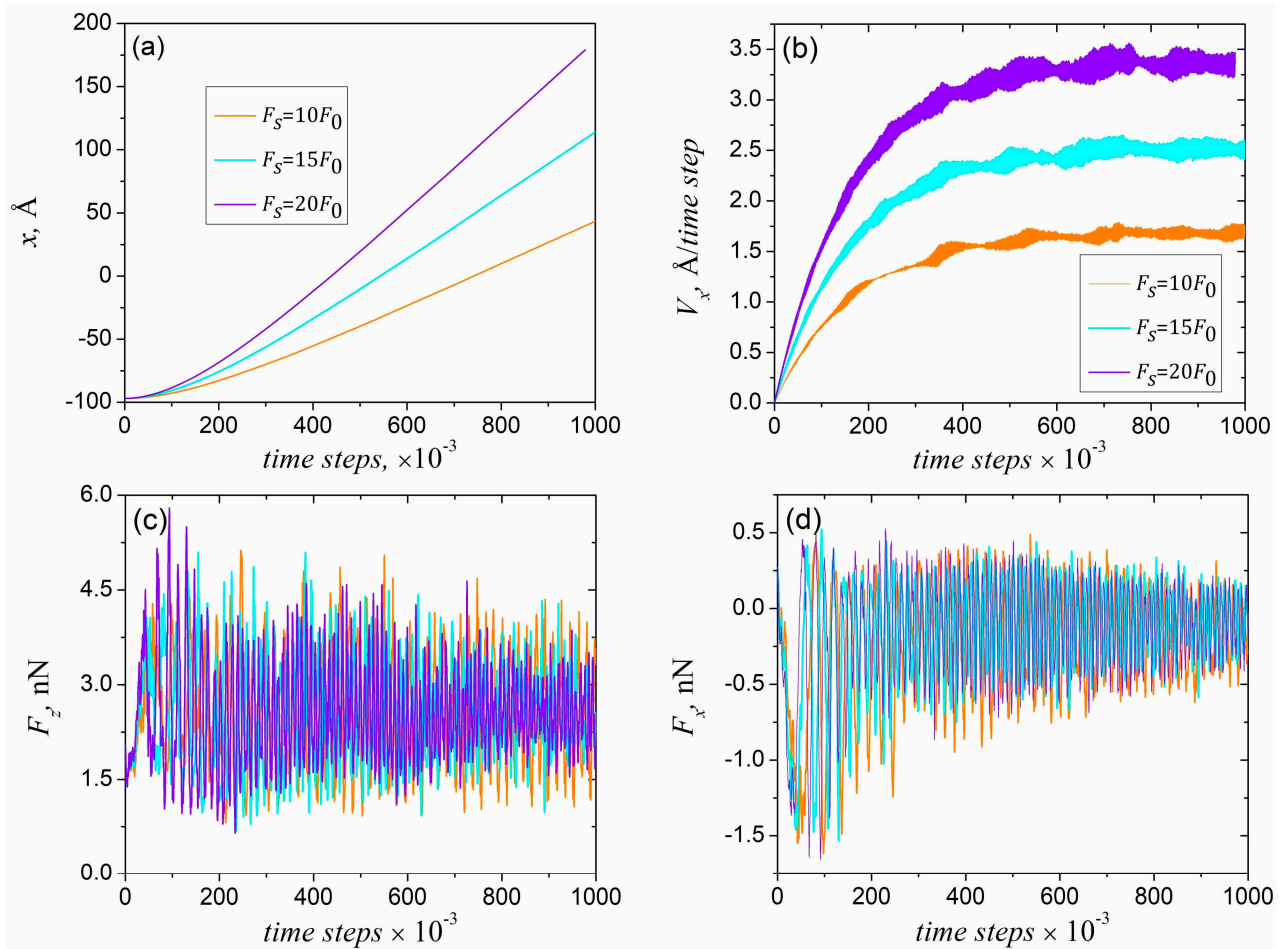


Figure 4. (a) Time dependencies of the average x coordinate of the nanoparticle under the external shear force of different magnitudes in $+x$ direction (values of applied force are shown in the figure). (b) Time dependencies of the x components of NP velocities, obtained from coordinates from panel (a). (c,d) Time dependencies of the normal F_z and tangential F_x forces acting on the nanoparticle from the substrate during the external load for all three experiments. Legend and coloring are the same for all panels. Supplementary Video S2 is available.

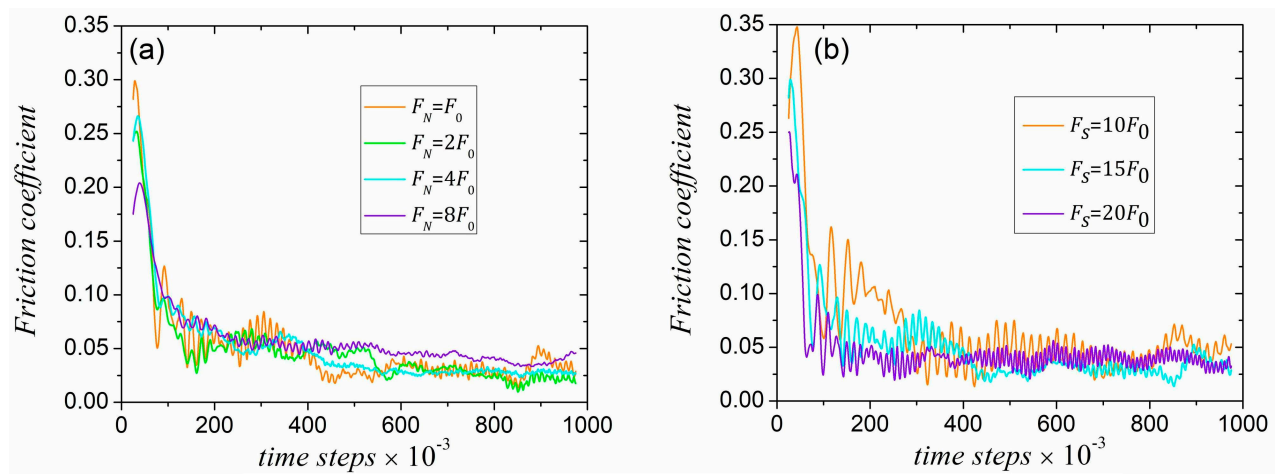


Figure 5. (a) Average friction coefficients calculated for experiments with different magnitudes of the normal load $F_N = F_0, 2F_0, 4F_0,$ and $8F_0$. (b) Average friction coefficients calculated for experiments with different shear forces $F_s = 10F_0, 15F_0,$ and $20F_0$ (magnitudes of the external forces are shown in the figures).

In addition, to investigate how the flexibility of the substrate affected the tribological properties of the system, we performed two experiments with different boundary conditions. Namely, Ti atoms in the bottom plane of the MXene were also allowed to move along the z axis. In this case, the application of the external load to the silver nanoparticle in the $-z$ direction together with the growth in the contact area also led to a vertical shift in the NP and a corresponding local deflection of the substrate. Figure 6a shows the time dependencies of the calculated size of the contact area under the external load and the corresponding time dependence of the average z coordinate of the Ag nanoparticle. Snapshots of the atomistic configuration of the system that demonstrate the local deflection of the substrate and the vertical shift in the nanoparticle are presented in Figure 6b.

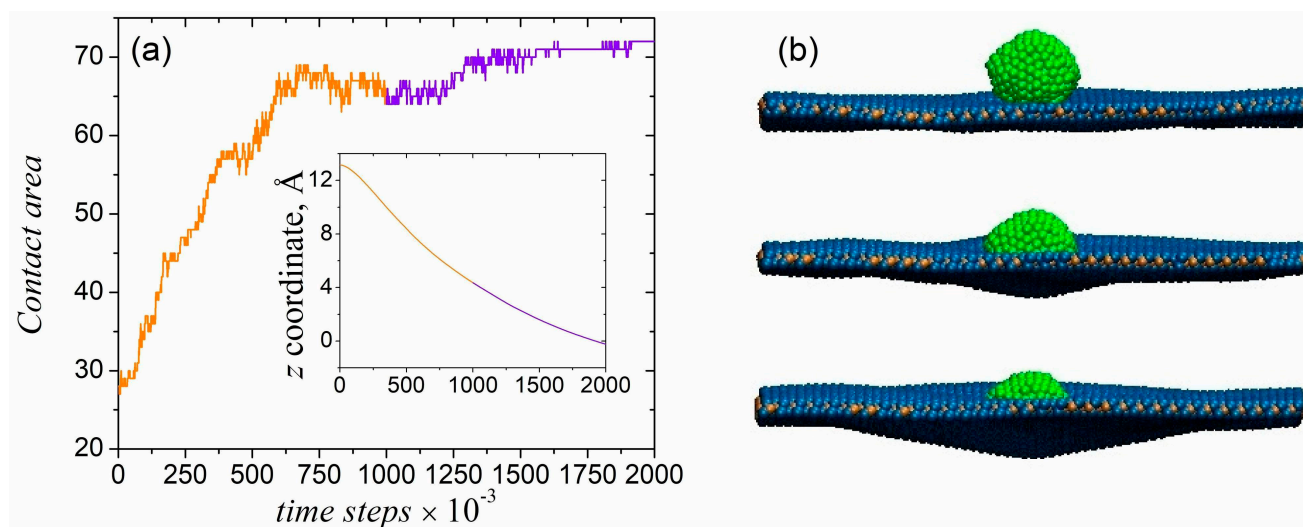


Figure 6. (a) Time dependence of the contact area between nanoparticle and the flexible substrate during the application of external load in normal direction (inset shows related time dependence of the average z coordinate of the NP). (b) Snapshots of the atomistic configurations of the system taken at the beginning of experiment ($t = 0$), at the end of first part ($t = 10^6$ time steps), and at the end of second part ($t = 2 \times 10^6$ time steps) from top to bottom. Dependencies related to the first and second parts of the experiment are denoted by different colors.

The size of the contact area increased fast during the first 7×10^5 time steps and changed insignificantly during the remaining time of the experiment. At the same time, as follows from the $z(t)$ dependence and the atomistic configurations of the system, deflection of the substrate and shifting of the nanoparticle were observed during the whole simulation time.

In the experiments concerning the sliding friction on the flexible substrate, two initial configurations of the system were considered, namely, after the external normal load was applied to the NP for 10^6 and 2×10^6 time steps. The selected configurations were related to the magnitudes of the vertical shift in the NP of 8 Å and 12 Å (see Figure 6). Different initial configurations were chosen to investigate how the initial deflection of the substrate affected the friction processes in the system. After the application of the normal load for a selected period of time, an external shear force $F_s = 15F_0$ was applied to the nanoparticle.

In contrast to the previous cases with a rigid substrate, sliding of the NP caused folding of the MXene ahead of the moving nanoparticle and the formation of wrinkles on its surface. Snapshots of the atomistic configurations that illustrate the described process in the experiment with the first initial configuration (with a smaller vertical shift in the NP) are shown in Figure 7.

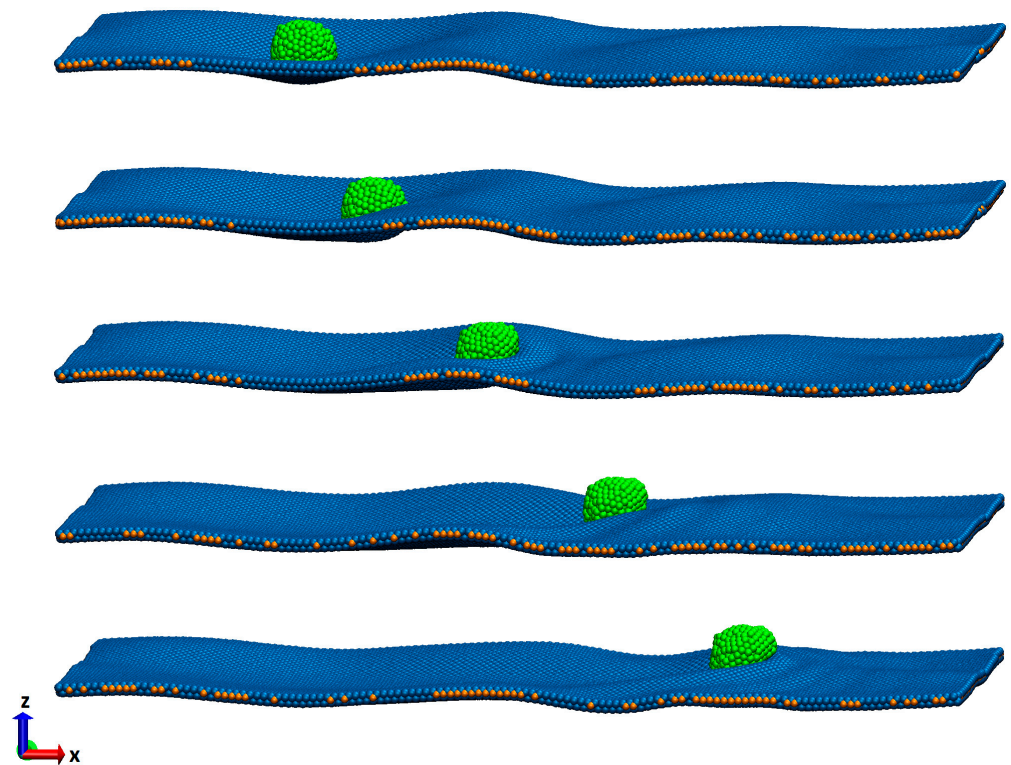


Figure 7. Snapshots of the atomistic configuration of the system during the sliding of the nanoparticle under external normal and shear forces on the flexible substrate.

The calculated time dependencies of the normal and tangential components of the forces acting on the nanoparticle from the substrate, the size of the contact areas, and the averaged friction coefficients for both the performed experiments are shown in Figure 8. As follows from the presented data, the time dependencies of the calculated friction force almost overlapped in the opening and final part of the experiment. However, the case with a smaller initial deflection of the substrate was characterized by lower magnitudes of both the friction force and the response from the substrate in the range of 2×10^5 – 6×10^5 time steps (see Figure 8a,b). During this time period, the difference between sizes of the contact area was also larger than in the opening and final parts of the experiment (Figure 8c). The calculated average values of the friction coefficient, shown in Figure 8d, exhibited similar behavior to the dependencies shown in Figure 8c, where the curve related to a smaller initial deflection reached its minimum at around $t = 6 \times 10^5$ time steps.

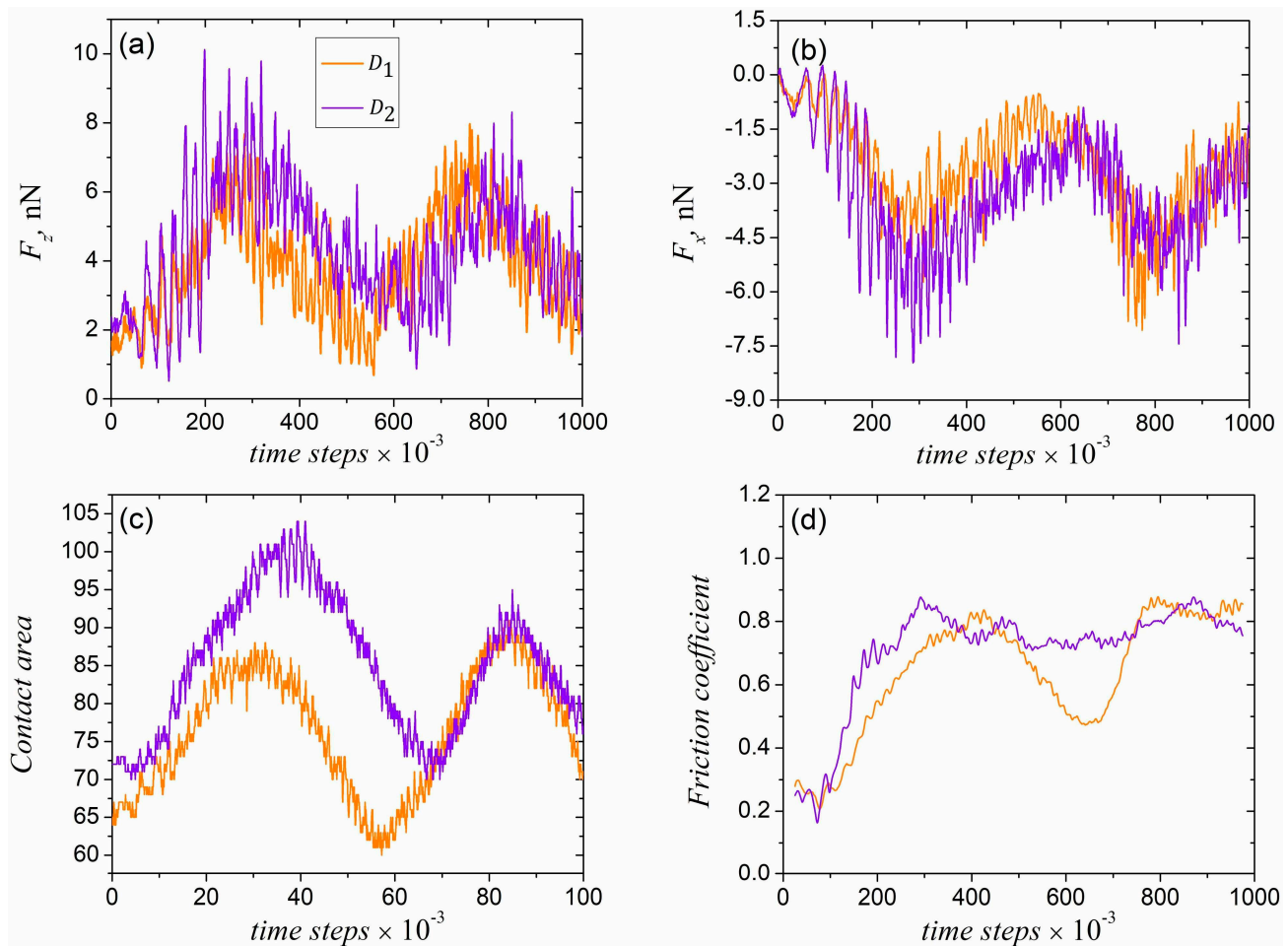


Figure 8. (a,b) Time dependencies of the normal F_z and tangential F_x forces acting on the nanoparticle from the flexible substrate during the external load calculated in experiments with different initial indentation depths of $D_1 = 8\text{\AA}$ and $D_2 = 12\text{\AA}$. (c,d) Time dependencies of the contact area size and friction coefficient between the NP and the substrate during sliding. Legend and coloring are the same for all panels.

4. Conclusions

We reported the results of computer experiments concerning the sliding of a silver nanoparticle on the surface of a Ti_2C substrate that were performed within classical molecular dynamics methods. Similar to typical experiments on friction performed with classic tribometers, we measured the friction force that occurred in the system under an external load. As follows from the data presented in the previous section, the experiments with different magnitudes of the normal and shear external force performed with rigid substrate were characterized by close values of the average friction coefficients. This property of the system, where the friction force is proportional to the applied load and is independent of the size of the contact area and sliding velocity, is known as the Amontons–Coulomb laws of friction. Thus, we may conclude that the performed simulations were physically correct and recreated basic tribological properties. Moreover, as follows from the data presented in Figure 8, the tribological properties of the system also slightly depended on the initial deflection of the substrate before the start of the motion of the nanoparticle. However, the friction coefficients calculated for friction of the NP on a flexible substrate exceeded the values obtained in the experiments with a rigid substrate by almost 10 times (see Figures 5 and 8d). Such a significant difference may be explained by the presence of wrinkles and folds on the surface in the first case. These formations on the surface of the substrate acted as additional obstacles that could hinder the motion of the nanoparticle, re-

sulting in greater interactions forces between the NP and the substrate and a corresponding growth of the friction coefficients.

It is worth noting that as we used empirically defined parameters of the interatomic potentials, the computed characteristics of the system may only be considered as qualitative rather than quantitative, and the obtained numerical data require further experimental and theoretical verification. Nevertheless, the calculated average values of the friction coefficients, μ , were within the range of approximately 0.02–0.05 (see Figure 5), which is close to the value of $\mu = 0.065$ measured in experiments between MXene/graphene oxide nanocomposites and rough steel surfaces reported in [44]. At the same time, the friction coefficient between MXenes and other two-dimensional materials are significantly lower ($\mu < 0.01$) [45]. Moreover, as was reported in [46], it is possible to achieve a superlubric regime for Ti_3C_2 MXene in a dry nitrogen environment. However, molecular dynamics simulations do not necessarily reproduce exact numerical parameters of the studied system; therefore, the obtained values can be only considered as approximate values that are valid for the particular studied system. Nevertheless, the performed experiment provides qualitative insights into the processes that occur at an atomistic level during friction between nanomaterials and may become useful in further studies in various areas of nanotribology.

Supplementary Materials: The following supporting information can be downloaded at: <https://www.mdpi.com/article/10.3390/cryst14030272/s1>, Video S1: Animation of the nanoparticle behavior under the external normal load. Top panels show evolution of the atomistic configuration of the NP (top left) and contact area (top right) under normal load (substrate atoms that are in contact are shown in red color). Bottom panels show corresponding time dependencies of the normal force acting from the substrate to the NP (bottom left) and contact area (bottom right). Presented animation is related to the dependencies $F_N = 4F_0$ in Figure 2. Video S2: Animation of the nanoparticle behavior under the external normal load and shear force. Top panels show evolution of the atomistic configuration of the NP (top left) and contact area (top right) under normal load and shear force (substrate atoms that are in contact are shown in red color). Bottom panels show related time dependencies of the NP velocity (bottom left) and contact area (bottom right). Presented animation is related to the dependencies $F_N = 4F_0$ in Figures 3 and 5. Data S3: Description of the interatomic potentials used in simulations.

Author Contributions: Supervision, project administration, writing—review and editing, V.L.P.; data interpretation, visualization (supplementary videos), writing—review and editing, I.A.L.; conceptualization, methodology, software, simulation, data analysis, visualization, writing—original draft preparation, V.B. All authors have read and agreed to the published version of the manuscript.

Funding: This work was supported in part by the German Academic Exchange Service (DAAD).

Data Availability Statement: The datasets generated for this study are available on request to the corresponding authors.

Conflicts of Interest: The authors declare no conflicts of interest.

References

1. Hirano, M. *Friction at the Atomic Level: Atomistic Approaches in Tribology*; Wiley-VCH: Weinheim, Germany, 2018. [CrossRef]
2. Müser, M.H. Towards an atomistic understanding of solid friction by computer simulations. *Comput. Phys. Commun.* **2002**, *146*, 54–62. [CrossRef]
3. He, Y.; She, D.; Liu, Z.; Wang, X.; Zhong, L.; Wang, C.; Wang, G.; Mao, S.X. Atomistic observation on diffusion-mediated friction between single-asperity contacts. *Nat. Mater.* **2022**, *21*, 173–180. [CrossRef] [PubMed]
4. Craighead, H.G. Nanoelectromechanical Systems. *Science* **2000**, *290*, 1532–1535. [CrossRef] [PubMed]
5. Ekinici, K.L.; Roukes, M.L. Nanoelectromechanical systems. *Rev. Sci. Instrum.* **2005**, *76*, 061101. [CrossRef]
6. Leidens, L.M.; Michels, A.F.; Perotti, B.L.; Alvarez, F.; Zanatta, A.R.; Figueroa, C.A. Nanotribology of Hydrogenated Amorphous Silicon: Sliding-Dependent Friction and Implications for Nanoelectromechanical Systems. *ACS Appl. Nano Mater.* **2022**, *5*, 15546–15556. [CrossRef]
7. Ferrari, P.F.; Kim, S.; van der Zande, A.M. Dissipation from Interlayer Friction in Graphene Nanoelectromechanical Resonators. *Nano Lett.* **2021**, *21*, 8058–8065. [CrossRef]
8. Ferrari, P.F.; Kim, S.; van der Zande, A.M. Nanoelectromechanical systems from two-dimensional materials. *Appl. Phys. Rev.* **2023**, *10*, 031302. [CrossRef]

9. Rasuli, H.; Rasuli, R. Nanoparticle-decorated graphene/graphene oxide: Synthesis, properties and applications. *J. Mater. Sci.* **2023**, *58*, 2971–2992. [[CrossRef](#)]
10. Kravchenko, Y.O.; Taran, A.; Shvets, U.S.; Kubakh, M.; Borysiuk, V. Atomistic Simulation of Ti₂C MXene Decoration with Ag Nanoparticles. *J. Nano-Electron. Phys.* **2023**, *15*, 02030. [[CrossRef](#)]
11. Gaboardi, M.; Bliersbach, A.; Bertoni, G.; Aramini, M.; Vlahopoulou, G.; Pontiroli, D.; Mauron, P.; Magnani, G.; Salviati, G.; Züttel, A.; et al. Decoration of graphene with nickel nanoparticles: Study of the interaction with hydrogen. *J. Mater. Chem. A* **2014**, *2*, 1039–1046. [[CrossRef](#)]
12. Rattan, S.; Kumar, S.; Goswamy, J.K. Gold nanoparticle decorated graphene for efficient sensing of NO₂ gas. *Sens. Int.* **2022**, *3*, 100147. [[CrossRef](#)]
13. Liang, X.; Liang, B.; Pan, Z.; Lang, X.; Zhang, Y.; Wang, G.; Yin, P.; Guo, L. Tuning plasmonic and chemical enhancement for SERS detection on graphene-based Au hybrids. *Nanoscale*. **2015**, *7*, 20188–20196. [[CrossRef](#)] [[PubMed](#)]
14. Mukherjee, S.; Bytesnikova, Z.; Martin, S.; Svec, P.; Ridoskova, A.; Pekarkova, J.; Seguin, C.; Weickert, J.-L.; Messaddeq, N.; Mély, Y.; et al. Silver Nanoparticle-Decorated Reduced Graphene Oxide Nanomaterials Exert Membrane Stress and Induce Immune Response to Inhibit the Early Phase of HIV-1 Infection. *Adv. Mater. Interfaces* **2023**, *10*, 2201996. [[CrossRef](#)]
15. You, Z.; Qiu, Q.; Chen, H.; Feng, Y.; Wang, X.; Wang, Y.; Ying, Y. Laser-induced noble metal nanoparticle-graphene composites enabled flexible biosensor for pathogen detection. *Biosens. Bioelectron.* **2020**, *150*, 111896. [[CrossRef](#)] [[PubMed](#)]
16. Li, L.; Zhang, N.; Zhang, M.; Wu, L.; Zhang, X.; Zhang, Z. Ag Nanoparticles Decorated 2D Titanium Carbide (MXene) with Superior Electrochemical Performance for Supercapacitors. *ACS Sustainable Chem. Eng.* **2018**, *6*, 7442–7450. [[CrossRef](#)]
17. Satheeshkumar, E.; Makaryan, T.; Melikyan, A.; Minassian, H.; Gogotsi, Y.; Yoshimura, M. One-step Solution Processing of Ag, Au and Pd@MXene Hybrids for SERS. *Sci. Rep.* **2016**, *6*, 32049. [[CrossRef](#)] [[PubMed](#)]
18. Gogotsi, Y.; Anasori, B. The Rise of MXenes. *ACS Nano* **2019**, *13*, 8491–8494. [[CrossRef](#)]
19. Anasori, B.; Lukatskaya, M.; Gogotsi, Y. 2D metal carbides and nitrides (MXenes) for energy storage. *Nat. Rev. Mater.* **2017**, *2*, 16098. [[CrossRef](#)]
20. Anasori, B.; Gogotsi, Y. *2D Metal Carbides and Nitrides (MXenes), Structure, Properties and Applications*; Springer: Berlin, Germany, 2019. [[CrossRef](#)]
21. Israelachvili, J.N.; Tabor, D. The Measurement of Van Der Waals Dispersion Forces in the Range 1.5 to 130 nm. *Proc. Math. Phys. Eng. Sci.* **1972**, *331*, 19–38.
22. Rosenkranz, A.; Righi, M.C.; Sumant, A.V.; Anasori, B.; Mochalin, V.N. Perspectives of 2D MXene Tribology. *Adv. Mater.* **2023**, *35*, 2207757. [[CrossRef](#)]
23. Lyashenko, I.A.; Borysiuk, V.N.; Manko, N.N. Statistical analysis of self-similar behaviour in the shear induced melting model. *Condens. Matter Phys.* **2014**, *17*, 23003. [[CrossRef](#)]
24. Rapaport, D.C. *The Art of Molecular Dynamics Simulation*; Cambridge University Press: Cambridge, UK, 2004. [[CrossRef](#)]
25. Sørensen, M.R.; Jacobsen, K.W.; Stoltze, P. Simulations of atomic-scale sliding friction. *Phys. Rev. B* **1996**, *53*, 2101. [[CrossRef](#)] [[PubMed](#)]
26. Wang, S.; Komvopoulos, K. A molecular dynamics study of the oxidation mechanism, nanostructure evolution, and friction characteristics of ultrathin amorphous carbon films in vacuum and oxygen atmosphere. *Sci. Rep.* **2021**, *11*, 3914. [[CrossRef](#)] [[PubMed](#)]
27. Hakala, T.J.; Holmberg, K.; Laukkanen, A. Coupling Molecular Dynamics and Micromechanics for the Assessment of Friction and Damage Accumulation in Diamond-Like Carbon Thin Films under Lubricated Sliding Contacts. *Lubricants* **2021**, *9*, 30. [[CrossRef](#)]
28. Gzik-Szumiatka, M.; Szumiatka, T.; Morozow, D.; Szewczyk, R. Elementary, Atomic-Level Friction Processes in Systems with Metallic Inclusions—Systematic Simulations for a Wide Range of Local Pressures. *Materials* **2021**, *14*, 4351. [[CrossRef](#)]
29. Harrison, J.A.; White, C.T.; Colton, R.J.; Brenner, D.W. Molecular-dynamics simulations of atomic-scale friction of diamond surfaces. *Phys. Rev. B* **1992**, *46*, 9700. [[CrossRef](#)]
30. Khomenko, A.V.; Prodanov, N.K. Study of Friction of Ag and Ni Nanoparticles: An Atomistic Approach. *J. Phys. Chem. C* **2010**, *114*, 19958–19965. [[CrossRef](#)]
31. Humphrey, W.; Dalke, A.; Schulten, K. VMD: Visual molecular dynamics. *J. Mol. Graph.* **1996**, *14*, 33–38. [[CrossRef](#)]
32. Borysiuk, V.; Mochalin, V.N. Thermal stability of two-dimensional titanium carbides Tin+1Cn (MXenes) from classical molecular dynamics simulations. *MRS Commun.* **2019**, *9*, 203–208. [[CrossRef](#)]
33. Oymak, H.; Erkoc, F. Titanium coverage on a single-wall carbon nanotube: Molecular dynamics simulations. *Chem. Phys.* **2004**, *300*, 277–283. [[CrossRef](#)]
34. Branco, D.d.C.; Cheng, G.J. Employing Hybrid Lennard-Jones and Axilrod-Teller Potentials to Parametrize Force Fields for the Simulation of Materials' Properties. *Materials* **2021**, *14*, 6352. [[CrossRef](#)]
35. Axilrod, B.M.; Teller, E. Interaction of the van der Waals type between three atoms. *J. Chem. Phys.* **1943**, *11*, 299. [[CrossRef](#)]
36. Zhou, X.W.; Wadley, H.N.G.; Johnson, R.A.; Larson, D.J.; Tabat, N.; Cerezo, A.; Petford-Long, A.K.; Smith, G.D.W.; Clifton, P.H.; Martens, R.L.; et al. Atomic scale structure of sputtered metal multilayers. *Acta Mater.* **2001**, *49*, 4005–4015. [[CrossRef](#)]
37. Sasaki, N.; Kobayashi, K.; Tsukada, M. Atomic-scale friction image of graphite in atomic-force microscopy. *Phys. Rev. B* **1996**, *54*, 2138. [[CrossRef](#)] [[PubMed](#)]
38. Anderson, J.A.; Lorenz, C.D.; Travesset, A. General purpose molecular dynamics simulations fully implemented on graphics processing units. *J. Comput. Phys.* **2008**, *227*, 5342–5359. [[CrossRef](#)]

39. van Meel, J.A.; Arnold, A.; Frenkel, D.; Zwart, S.F.P.; Belleman, R.G. Harvesting graphics power for MD simulations. *Mol. Simul.* **2008**, *34*, 259–266. [[CrossRef](#)]
40. Berendsen, H.J.C.; Postma, J.P.M.; van Gunsteren, W.F.; DiNola, A.; Haak, J.R. Molecular-Dynamics with Coupling to an External Bath. *J. Chem. Phys.* **1984**, *81*, 3684. [[CrossRef](#)]
41. Lyashenko, I.A.; Popov, V.L.; Pohrt, R.; Borysiuk, V. High-Precision Tribometer for Studies of Adhesive Contacts. *Sensors* **2023**, *23*, 456. [[CrossRef](#)] [[PubMed](#)]
42. Lyashenko, I.A.; Khomenko, A.V.; Metlov, L.S. Nonlinear thermodynamic model of boundary friction. *J. Frict. Wear* **2011**, *32*, 113–123. [[CrossRef](#)]
43. Lyashenko, I.A.; Khomenko, A.V.; Zaskoka, A.M. Hysteresis Behavior in the Stick-Slip Mode at the Boundary Friction. *Tribol. Trans.* **2013**, *56*, 1019–1026. [[CrossRef](#)]
44. Macknoja, A.Z.; Ayyagari, A.; Shevchenko, E.; Berman, D. MXene/graphene oxide nanocomposites for friction and wear reduction of rough steel surfaces. *Sci. Rep.* **2023**, *13*, 11057. [[CrossRef](#)] [[PubMed](#)]
45. Li, Y.; Huang, S.; Wei, C.; Zhou, D.; Li, B.; Mochalin, V.N.; Chenglin Wu, C. Friction between MXenes and other two-dimensional materials at the nanoscale. *Carbon* **2022**, *196*, 774–782. [[CrossRef](#)]
46. Huang, S.; Mutyala, K.C.; Sumant, A.V.; Mochalin, V.N. Achieving superlubricity with 2D transition metal carbides (MXenes) and MXene/graphene coatings. *Mater. Today Adv.* **2021**, *9*, 100133. [[CrossRef](#)]

Disclaimer/Publisher’s Note: The statements, opinions and data contained in all publications are solely those of the individual author(s) and contributor(s) and not of MDPI and/or the editor(s). MDPI and/or the editor(s) disclaim responsibility for any injury to people or property resulting from any ideas, methods, instructions or products referred to in the content.